Neuro-Oncology Advances

6(1), 1–14, 2024 | https://doi.org/10.1093/noajnl/vdae005 | Advance Access date 25 January 2024

Single-nucleus expression characterization of non-enhancing region of recurrent high-grade glioma

Kunal S. Patel[†], Kaleab K. Tessema[†], Riki Kawaguchi, Lindsey Dudley, Alvaro G. Alvarado, Sree Deepthi Muthukrishnan, Travis Perryman, Akifumi Hagiwara, Vivek Swarup, Linda M. Liau, Anthony C. Wang, William Yong, Daniel H. Geschwind, Ichiro Nakano, Steven A. Goldman, Richard G. Everson[‡], Benjamin M. Ellingson[‡], and Harley I. Kornblum[‡]

Department of Neurosurgery, David Geffen School of Medicine at UCLA, Los Angeles, California, USA (K.S.P., L.M.L., A.C.W., R.G.E., B.M.E.); The Intellectual and Developmental Disabilities Research Center and Department of Psychiatry and Biobehavioral Sciences, David Geffen School of Medicine at UCLA, Los Angeles, California, USA (K.K.T., L.D., A.G.A., S.D.M., H.I.K.); Department of Neurology, David Geffen School of Medicine at UCLA, Los Angeles, California, USA (R.K., D.H.G.); UCLA Brain Tumor Imaging Laboratory (BTIL), Department of Radiological Sciences, David Geffen School of Medicine at UCLA, Los Angeles, California, USA (A.H., B.M.E.); Department of Neurobiology and Behavior, UCI School of Biological Sciences, Irvine, California, USA (V.S.); Department of Pathology, David Geffen School of Medicine at UCLA, Los Angeles, California, USA (W.Y.); Department of Neurosurgery, Hokuto Social Medical Corporation, Hokuto Hospital, Hokuto, Japan (I.N.); Center for Translational Neuromedicine, University of Rochester Medical Center, Rochester, New York, USA (S.A.G.); Faculty of Health and Medical Sciences, Center for Translational Neuromedicine, University of Copenhagen, Copenhagen, Denmark (S.A.G.); Department of Radiation Oncology, David Geffen School of Medicine at UCLA, Los Angeles, California, USA (R.G.E.); Departments of Pediatrics, Psychiatry, and Molecular and Medical Pharmacology, David Geffen School of Medicine at UCLA, Los Angeles, California, USA (H.I.K.)

[†]These authors contributed equally to this work.

[‡]These authors jointly supervised this work.

Corresponding Author: Harley I. Kornblum, MD, PhD, Departments of Pediatrics, Psychiatry, and Molecular and Medical Pharmacology, David Geffen School of Medicine at UCLA, NRB Room 375D, 635 Charles E. Young Drive South, Los Angeles, CA 90095, USA (hkornblum@mednet.ucla.edu).

Abstract

Background. Non-enhancing (NE) infiltrating tumor cells beyond the contrast-enhancing (CE) bulk of tumor are potential propagators of recurrence after gross total resection of high-grade glioma.

Methods. We leveraged single-nucleus RNA sequencing on 15 specimens from recurrent high-grade gliomas ($n = 5$) to compare prospectively identified biopsy specimens acquired from CE and NE regions. Additionally, 24 CE and 22 NE biopsies had immunohistochemical staining to validate RNA findings.

Results. Tumor cells in NE regions are enriched in neural progenitor cell-like cellular states, while CE regions are enriched in mesenchymal-like states. NE glioma cells have similar proportions of proliferative and putative glioma stem cells relative to CE regions, without significant differences in % Ki-67 staining. Tumor cells in NE regions exhibit upregulation of genes previously associated with lower grade gliomas. Our findings in recurrent GBM paralleled some of the findings in a re-analysis of a dataset from primary GBM. Cell-, gene-, and pathway-level analyses of the tumor microenvironment in the NE region reveal relative downregulation of tumor-mediated neovascularization and cell-mediated immune response, but increased glioma-to-nonpathological cell interactions.

Conclusions. This comprehensive analysis illustrates differing tumor and nontumor landscapes of CE and NE regions in high-grade gliomas, highlighting the NE region as an area harboring likely initiators of recurrence in a pro-tumor microenvironment and identifying possible targets for future design of NE-specific adjuvant therapy. These findings also support the aggressive approach to resection of tumor-bearing NE regions.

Key Points

- Significant proliferating tumor burden exists in non-enhancing regions of glioma.
- Non-enhancing regions have unique tumor and nontumor expression profiles.

Importance of the Study

Standard-of-care treatment for glioblastoma relies on visualization of tumor via contrast-enhanced magnetic resonance imaging. However, non-enhancing regions harbor tumor cells that should be targets for adjuvant therapy, given these regions are not resected in surgery. To begin addressing these infiltrating non-enhancing tumor cells, we thoroughly characterize the tumor and nontumor microenvironment of non-enhancing regions in high-grade gliomas. Understanding the total tumor burden, proliferating tumor ratio, and presence of putative glioma stem cells may help design adjuvant therapies for this unique population of tumor cells. Understanding the nontumor immune and vascular microenvironment may help target these areas via drug delivery and immunotherapy. Overall, in a disease marked by significant intratumoral heterogeneity, we focus on identifying therapeutic strategies for areas not addressed by surgery.

The intervention that contributes most to overall survival in adult glioma remains the surgical removal of tumors.[1,2] The current surgical standard of care is imaging-based resection of the contrast-enhancing (CE) region as depicted by gadolinium contrast-enhanced T1-weighted magnetic resonance imaging (MRI),[3] where increased extent of resection[4] and lower postsurgical residual enhancing disease[5] have been shown to be correlated with improved survival. However, despite total resection of the CE region, high-grade gliomas invariably recur, and this most commonly occurs at the edge of the resection cavity.[6]

Treatment options for recurrent malignant glioma include repeat resection, chemotherapy, molecular therapy,[7–9] immunotherapy,[10] or a combination of the above treatments. Given the modest, at best, efficacy in randomized trials, further study into treatment for recurrent glioma is needed. Strategies for molecularly targeted therapy for recurrent glioma have largely been developed by studying bulk RNA or protein expression from cell lines or clinical surgical specimens, which, as described above, generally derive from the CE portion of the tumor. This strategy (1) fails to account for cellular heterogeneity and (2) ignores the true targets of adjuvant therapy for glioma: the residual cells beyond the CE region that are not resected. While more recent studies have utilized single-cell sequencing to study intratumoral heterogeneity,[11–18] they have largely focused on single samples from CE regions, yielding limited insight into infiltrating cells beyond the CE region and their clinical relevance. Furthermore, in addition to understanding infiltrating tumor cells, it is important to understand the nontumor microenvironment along with tumor–microenvironment interactions regulating immune response, vasculature, and normal nervous system function.[10]

In this study, we prospectively sample CE regions and tissue beyond the enhancing edge (non-enhancing, "NE") from 5 high-grade gliomas: 3 grade 4 IDH-wild-type glioblastomas, 1 grade 4 IDH-mutant astrocytoma, and 1 grade 3 IDH-mutant oligodendroglioma. We couple intraoperative neuronavigation-guided targeting of biopsy specimens with single-nucleus RNA sequencing (snRNA-seq) to comprehensively characterize region-specific cellular and molecular features. Our experimental design differs from previous single-cell analyses in glioma in that we leverage prospectively determined positional data to model the spatial landscape of cell populations within CE and NE regions, producing an improved[19] yield of single-cell data from NE regions of tumor. We perform a comprehensive single-cell characterization of the NE region to assess tumor cell burden, composition of tumor and nontumor cells, molecular features of tumor and nontumor cells, and tumor–microenvironment interactions. These data provide an important description of the biological landscape of infiltrating tumor cells and identify potential targets for improved postoperative adjuvant therapy.

Methods

Lead Contact and Materials Availability

Please direct requests for further information and/or resources to Harley Kornblum (hkornblum@mednet.ucla.edu).

MRI-Guided Biopsy Targets in Human Gliomas

Patients with recurrent high-grade glioma were included in this study. We chose recurrent glioma given its clinical burden and limited single-cell analysis of recurrent glioma relative to primary glioma.[13] Each patient had a single previous resection with adjuvant temozolomide and radiation therapy only. While all patients had surgery for local recurrence, we were not able to acquire previous radiation plans to identify whether NE regions were included in the treatment plan. Patients referred to UCLA Neurosurgery

for intrinsic supratentorial brain tumors underwent 3 Tesla thin-cut preoperative MRI (3T Siemens Prisma, Siemens Healthcare, Erlangen, Germany) with and without gadolinium contrast (gadopentetate dimeglumine; Magnevist; Bayer HealthCare Pharmaceuticals) according to the international standardized brain tumor imaging protocol[20] within 1 week of surgery. Images of the following sequences were downloaded: T1 3-dimensional magnetization-prepared rapid gradient echo (MP-RAGE) with and without contrast. Using AFNI, software for analysis and visualization of functional magnetic resonance neuroimages,[21] three 5 mm × 5 mm × 5 mm spherical biopsy targets were selected per patient by a multidisciplinary team (neurosurgery, neuroradiology, and neuro-oncology) based on feasibility and anatomic landmarks in order to minimize surgical inaccuracy from brain shift. Biopsy targets were then transferred to Brainlab Curve (BrainLAB AG, Munich, Germany), a surgical neuronavigation software, for intraoperative image guidance and tissue acquisition. There was no change to surgical and postsurgical standard-of-care therapy[22] for all patients. Specimens were immediately fresh frozen for nuclear isolation or paraffin-embedded for immunohistochemistry (IHC).

Immunohistochemistry Analysis

MRI-targeted biopsy specimens were collected from 17 patients with malignant glioma, yielding 22 specimens from NE regions and 24 from CE regions. Specimens were paraffin-embedded and stained with associated antibody (anti-Ki-67, anti-EGFR, anti-MBP, anti-NeuN, anti-CD8, anti-CD31, anti-CD155, anti-MAG, Abcam). Image-based quantification was done using QuPath[23] to calculate the percentage of sample pixels with positive staining. Samples were compared using independent samples *t*-tests as well as paired samples *t*-tests in the 5 patients from whom both CE and NE specimens were acquired.

Single-Nucleus RNA Sequencing (snRNA-seq) of Glioma Specimens

Single nuclei were isolated from frozen tumor specimens using iodixanol-based density gradient centrifugation and submitted to UCLA Technology Center for Genomics and Bioinformatics for library preparation and sequencing (Supplementary Methods, *Isolation of single nuclei from tumor specimens).* Single-nucleus cDNA libraries were generated using the Chromium Single Cell 3′ v3 kit (10x Genomics) and sequenced at 600 million reads/library and 2 × 50 base pairs using the NovaSeq 6000 S2 platform (Illumina). Raw reads were demultiplexed and Cell Ranger (10x Genomics) was used for alignment (human genome GRCh38), filtering, barcode identification, and counting of unique molecular identifiers, resulting in a feature-barcode (ie, gene-cell) matrix for each biopsy specimen (Supplementary Methods, *Single nucleus library preparation, sequencing, read alignment*). A second comparison set of single-cell transcriptomes from MRI-guided biopsies of CE and NE regions in newly diagnosed glioblastoma was downloaded and data were treated in a parallel fashion for all further steps (GSE84465).

SnRNA-seq Bioinformatic Processing and Analysis

Detailed methods are described in Supplementary Methods. Preprocessing, integration, and clustering were conducted using the R package Seurat[24–26] (Supplementary Methods, *SnRNA-seq integration and clustering*). To identify malignant cells in each patient dataset, we developed a multistep cell classification approach integrating both gene expression profiles and iterative prediction of copy number alteration (CNA) profiles (Supplementary Methods, *Streamlined CNA inference tool*). To identify nonmalignant cell types, we developed an improved tool for identifying cell types based on canonical cell type markers (Supplementary Methods, *Cell type marker visualization tool*). We used the integrated model of glioblastoma malignant cellular states[27] to classify glioma cellular states (Supplementary Methods, *Molecular classification of glioma cellular states*) and cycling cells (Supplementary Methods, *Identification of cycling cells*). We used previously described definitions of putative glioma stem cells (GSCs)[28–34] to label malignant cells as such (Supplementary Methods, *Identification of putative glioma stem cells*). Cell–cell communication analysis was performed using the CellChat package[35] (Supplementary Methods, *Cell-cell communication analysis*).

Estimating Extent of Tumor Burden

Cell type abundances from single-cell sequencing data were used to calculate the tumor cell burden at different biopsy sites. Tumor cell number was normalized by the nontumor oligodendrocyte number to control for total cells sequenced, which varied per sample. Segmentations of CE lesion of tumor were calculated using previously described methods.[36] Using AFNI,[21] this segmentation was minimized to obtain an ROI at the volumetric center of the lesion. The distance between the prospective biopsy ROI and this center of lesion ROI was calculated. The tumor:oligodendrocyte ratio was plotted against this distance. A quadratic model was implemented[37]:

$$x = \frac{-b \pm \sqrt{b^2 - 4ac}}{2a}$$

and x solved to identify the Y asymptote as the predicted distance from the center when the cell ratio approaches 0. A spherical heatmap ROI with a radius r equal to this distance was created and overlaid on T1 with contrast images.

$$V = \frac{4}{3}\pi r^3$$

Statistics

Statistical analysis was carried out in GraphPad Prism (GraphPad Software, San Diego, CA). Independent and paired *t*-tests and chi-square tests were used to evaluate

differences in tumor and nontumor cell quantities, cellular states, cell cycling proportions, and % positive Ki-67. Differential gene expression and pathway enrichment analyses underwent correction for multiple comparisons using the native functionality of the Seurat and fgsea packages, respectively. Significance was defined using an alpha level of 0.05 except as noted in the figures.

Study Approval

This study was approved by the UCLA IRB #10-000655 and #14-001261. All patients provided informed consent for all medical and surgical procedures and involvement in research studies.

Data Availability

Integrated data objects containing counts and metadata for both tumor cells and nontumor cells are available at the following Synapse project: https://www.synapse.org/NEvCE_snRNAseq_PatelTessema. Raw and processed sequencing data will be made available to the public through a GEO submission. Custom scripts for analysis and figure reproduction will be shared through the following GitHub repository: https://github.com/ktessema/PatelTessema_Glioma_NEvsCE_2023.

Results

Analysis of Human Recurrent Gliomas Using Single-Nucleus RNA Sequencing

We prospectively identified biopsy targets using preoperative MRI in 5 patients undergoing surgery for recurrent high-grade glioma (Table 1). All patients had previous resection and standard-of-care adjuvant temozolomide and radiation therapy only. We selected 2 biopsy targets from the CE region of each tumor and 1 from the non-enhancing (NE) region, located 5–20 mm from the CE edge (Figure 1A). Clinical pathology and fluorescence in situ hybridization identified 5 high-grade gliomas (3 grade 4 IDH-wild-type glioblastomas, 1 grade 4 IDH-mutant astrocytoma, 1 grade 3 IDH-mutant and 1p/19q co-deleted oligodendroglioma) (Table 1). We refer to these tumors as Gr4-GBM, Gr4-AST, and Gr3-ODG, respectively.[38] To analyze these tumors, we performed single-nucleus RNA sequencing (snRNA-seq) of 15 biopsy specimens (Figure 1B), yielding 32 914 individual transcriptomes that passed rigorous quality control and were included in subsequent analyses (Table 1, Figure 1C). Similarly, we identified a publicly available dataset using prospective guided biopsies in newly diagnosed glioblastoma (GSE84465, Supplementary Figure 1A).[19]

Significant Tumor Burden and Altered Malignant Cell Composition in the NE Regions of High-Grade Gliomas

We used MRI-based positional information to compare the CE and T2-hyperintense NE regions (Figure 2A). We first assessed tumor burden in the NE region by quantifying malignant cell proportions, revealing a notable malignant cell burden present in the NE region in all patients (15.3%–60.6% of NE cells; NE/CE malignant cell ratio of 0.58–1.13; Figure 2B). The presence of tumor cells in NE regions was also identified in the dataset of newly diagnosed GBM (8%, Supplementary Figure 1B). Given that malignant cells comprised a notable proportion of the NE regions, we sought to model the spatial extent of tumor burden on MRI. Using tumor cell quantity from 3 locations in 2 tumors, we applied a quadratic model (see Methods) to extrapolate the distance from the center of the tumor to where the tumor burden would approach 0 (Figure 2C). This model predicted tumor cell presence 4.94 and 2.31 cm, respectively, from the center of the tumor, and a spheroid with this radius was constructed and overlaid on the corresponding preoperative MR image (Figure 2D). The predicted tumor edge was beyond the CE region by 0.34–2.45 cm. While the invasion and growth patterns of glioma are complex, with cases of multifocal and distant lesions,[39] our data suggest a consistent presence of marked and potentially clinically significant tumor burden immediately surrounding the CE bulk.

We then examined malignant cellular states as described previously[27] across regions and noted significant heterogeneity in terms of cellular state composition (Figure 2E). NE regions harbored a higher NPC-like proportion (mean + 14%, paired *t*-test $P = .03$) and nonsignificantly trended toward a lower MES-like proportion (mean –15.0%, paired *t*-test $P = .12$), while AC- and OPC-like proportions were not consistently different. These trends were also

Table 1. Clinical, pathological, and sequencing characteristics of included samples

Sample	Age	Sex	Diagnosis	Grade	IDH^{mut}	1p/19q$^{-/-}$	EGFR^{+}	PTEN^{-}	MGMT^{+}	No. cells (pre-QC)	No. cells (post-QC)	Median genes/cell	Median UMI/cell
Gr4-GBM-1	65	M	GBM	IV	-	-	-	+	+	5563	3684	1780	3280
Gr4-GBM-2	69	M	GBM	IV	-	-	-	-	-	5540	4168	2701	6015
Gr4-GBM-3	77	M	GBM	IV	-	-	+	+	+	11115	7187	3145	6253
Gr4-AST	31	M	Astrocytoma	IV	+	-	-	-	-	4639	4153	3283	9059
Gr3-ODG	65	M	Oligodendroglioma	III	+	+	-	-	-	4935	4742	3817	10941

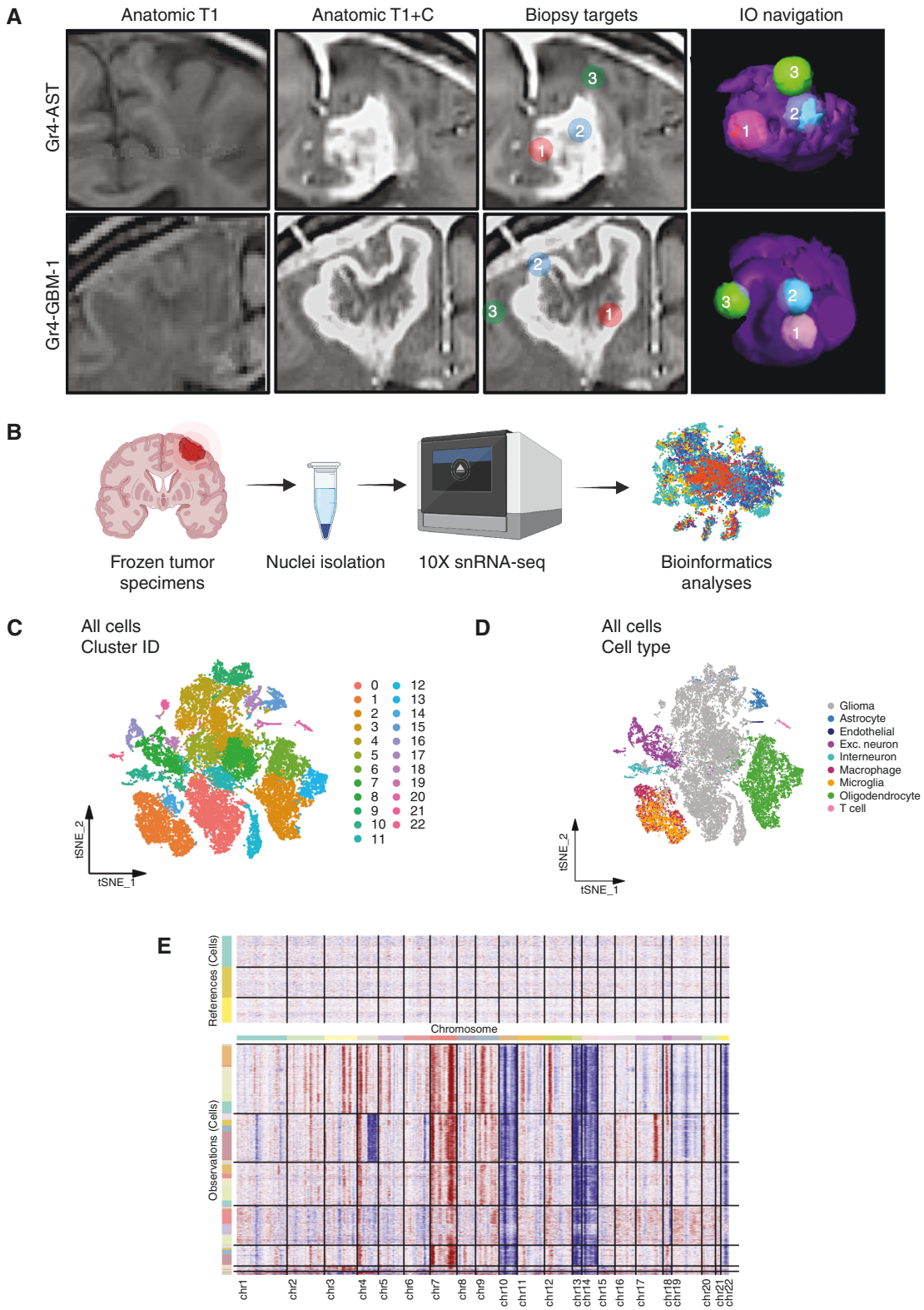

Figure 1. Single-nucleus RNA-sequencing analysis of MRI-guided glioma biopsy targets. (A) Preoperative targeted MRI: T1-weighted images without contrast (T1), with contrast (T1 + C), prospective biopsy targets, and intraoperative (IO) neuronavigation renderings of contrast-enhancing (target 1 and 2, inside CE lesion) and non-enhancing (target 3, outside CE lesion) samples. (B) Single-nucleus RNA-sequencing (snRNA-seq) experimental workflow. (C, D) Two-dimensional *t*-distributed stochastic neighbor embedding (t-SNE) plots showing the integrated snRNA-seq dataset with all sequenced nuclei (C) and annotated by cell type (D), and example of copy number variation analysis (E).

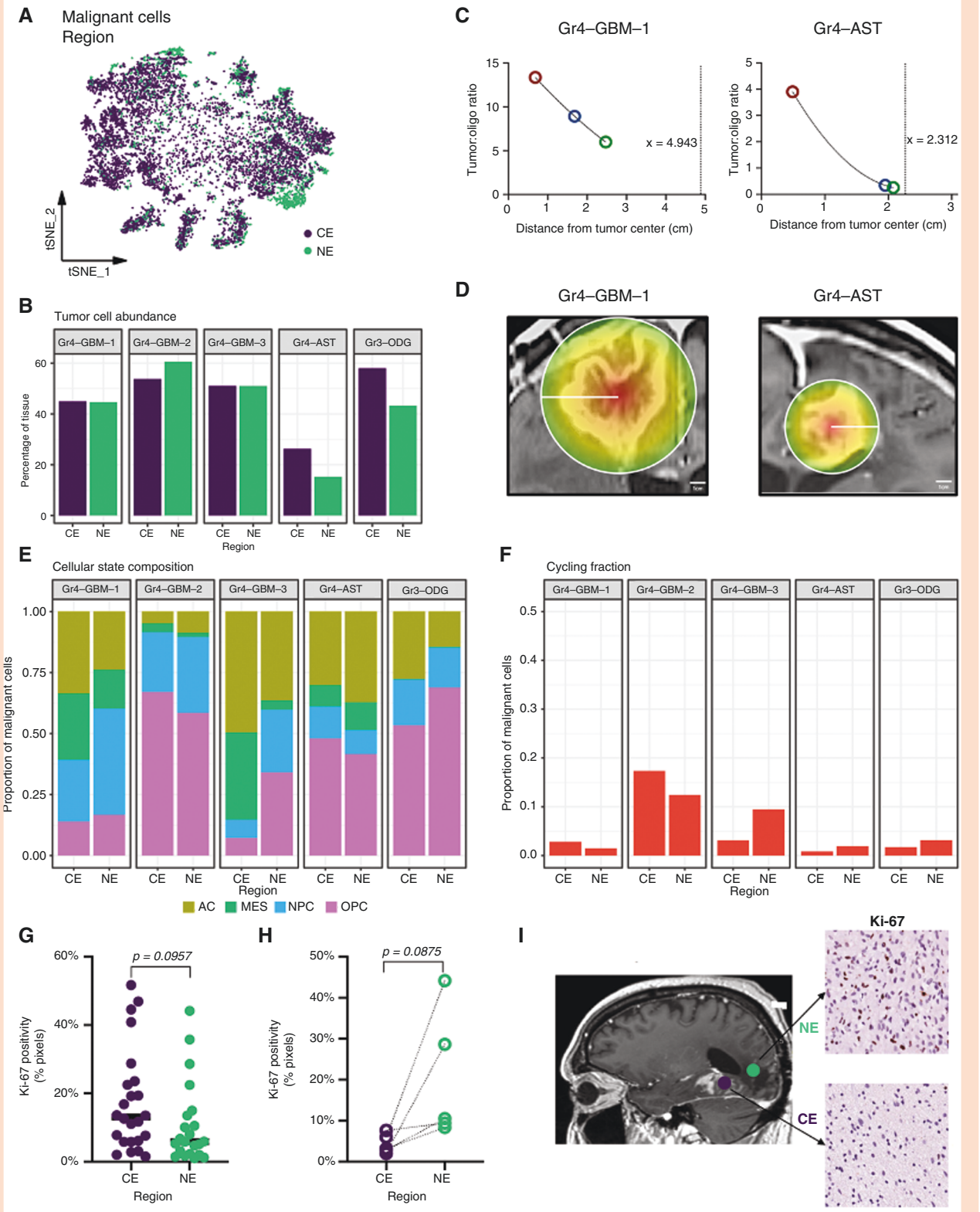

Figure 2. Characterizing tumor burden and composition in the non-enhancing region. (A) t-SNE plot of malignant cells from all patients, colored by biopsy region. (B) Quantification of tumor burden (proportion of all cells that are malignant) in the CE and NE regions of each tumor. (C, D) Tumor burden relative to distance from the tumor center was modeled for Gr4-GBM-1 and Gr4-AST. (C) Fitting the tumor cell:oligodendrocyte ratio to a quadratic curve (solid line), with the dotted line representing predicted distance (in centimeters) from the tumor center where tumor burden approaches 0. (D) Preoperative MR scan with superimposed heatmap of predicted tumor burden. (E, F) Malignant cellular state composition (E) and cycling cell fraction (F) in the CE and NE regions of each tumor. (G, H) Quantification of immunohistochemistry staining for Ki-67 stratified by region using nonpaired (G) and paired (H) biopsy samples. Statistical comparisons were performed using independent and paired *t*-tests, respectively. (I) Representative example of regions of Ki-67 staining in CE and NE regions.

seen in newly diagnosed GBM (Supplementary Figure 1B). IDH-mutant samples were further analyzed using cellular state signatures derived from IDH-mutant tumors (Supplementary Figure 2A and B).[12] This showed no difference between regions, although this analysis was limited by sample size. There was a cycling fraction in the NE regions of all tumors (Figure 2F), with no significant difference between regions (mean + 0.51% in NE, paired *t*-test $P = .792$). We also found evidence of cycling tumor cells in NE regions in newly diagnosed GBM (Supplementary Figure 1B). To further characterize tumor cell cycling via IHC, we obtained image-guided biopsies from an additional cohort of 17 patients with high-grade glioma and analyzed a total of 22 tissue specimens from NE regions and 24 from CE regions (Table 2). Quantification of Ki-67 staining showed a wide distribution in both regions, including several NE samples with high Ki-67 positivity, but no significant difference between regions ($P = .0957$, unpaired *t*-test; Figure 2G). We also analyzed paired samples from 5 patients with both regions sampled during the same procedure, with again no significant difference between regions ($P = .0875$, paired *t*-test; Figure 2H and I). Interestingly, we found that the cycling proportion of malignant cells in CE (but not NE) was predictive of tumor burden in NE ($P < .001$, Spearman's rho = 1). Together, these data indicate that there are ample numbers of proliferating tumor cells in the NE region, a potential etiology for recurrence.

Gene Expression and Pathway Enrichment Profiles in Malignant Cells From NE Regions

To investigate regional heterogeneity in malignant cell transcriptomes, we identified differentially expressed genes (DEGs) between regions (Figure 3A and B). Top NE-enriched DEGs (change >25% and adjusted $P < 1e^{-10}$) included genes associated with neuronal/synaptic function (eg, *TNR, NRXN1, ANKS1B, CADM2, IL1RAPL, PAK3, PLCL1, ERC2, SCN3A, KCN3*), genes upregulated in lower grade gliomas (eg, *TNR, GALANT13, TMEFF2, PAK3, SPOCK1*), and genes associated with immune-cold phenotypes (eg, *NRXN1*). Top CE-enriched DEGs included genes associated with metabolism (eg, *ABCA1, NAMPT*), proliferation/invasion (eg, *CD44, SPP1, IGFBP7, IGFBP5, RYR3, TNC*), and angiogenesis (eg, *VEGFA, IGFBP7, TNC*). To further determine the functional implications of NE-specific transcriptional patterns, DEGs were then used as input for gene set enrichment analysis (GSEA) with a combination of databases: Gene Ontology Biological Pathways, Canonical Pathways, Oncogenic Pathways, and Transcription Factor Targets. GSEA using conserved DEGs in malignant cells across tumors identified 686 differentially activated pathways in NE versus CE (Benjamini-Hochberg adjusted $P < .05$). The top 20 NE-enriched pathways (normalized enrichment score >2.0) were all related to neuronal/synaptic function, while the top 20 CE-enriched pathways included interferon-gamma signaling, growth factors, vasculature development, and extracellular matrix regulation. A similar analysis of differential expression in NE vs. CE using a separate dataset of newly diagnosed GBM yielded a >20% overlap in DEGs, with multiple genes enriched in NE or CE regions following the same trend in this additional dataset. Of the top 10 NE-enriched genes in our recurrent glioma dataset, 9 were also NE-enriched in this primary GBM dataset. The 10th, IL1TRAP, showed almost no expression in the NE in primary GBM (Supplementary Figure 1C and D). Taken together, our gene-, pathway-, and population-level analyses show significant differences between malignant cells in the NE and CE regions, suggesting CE regions are areas of rapid growth, angiogenesis, and inflammation,

Table 2. Patient cohort information for localized biopsy immunohistochemistry

Patient	Age	Gender	Grade	IDH mutation	1p/19q deletion	Region sampled
1	61	M	4	-	-	NE
2	35	M	4	-	-	NE
3	46	F	4	+	-	Both
4	59	M	4	-	-	Both
5	70	F	4	-	-	CE
6	29	M	3	+	-	Both
7	59	M	4	-	-	NE
8	49	M	3	+	-	NE
9	61	F	4	-	-	CE
10	53	M	4	-	-	Both
11	49	M	3	+	+	CE
12	70	M	4	-	-	NE
13	40	M	4	-	-	CE
14	59	F	4	-	-	Both
15	44	M	4	-	-	CE
16	39	M	3	+	+	CE
17	62	M	3	+	+	CE

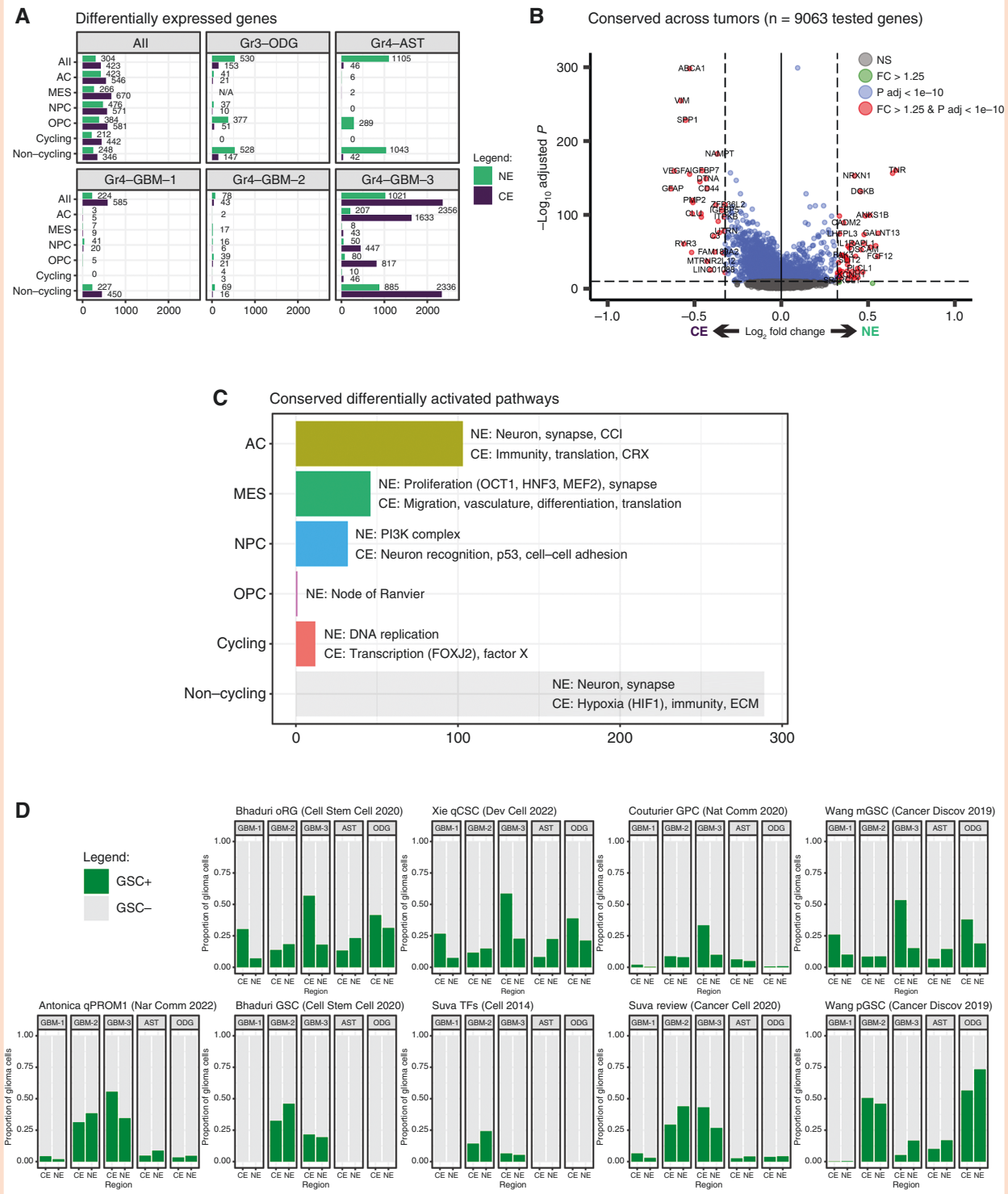

Figure 3. Region-specific molecular features of malignant cells in high-grade glioma. (A) Number of NE-enriched and CE-enriched differentially expressed genes (DEGs) in each tumor and malignant cell group. (B) Volcano plot showing malignant cell DEGs that are conserved across patients (all cell states combined). (C) Number and summary of significantly differentially activated pathways in NE versus CE identified in each cell group using gene set enrichment analysis (GSEA). DEGs conserved across patients were used as input. The list of tested pathways was a combination of GO Biological Process, Canonical Pathway, Oncogenic Pathway, and Transcription Factor Target databases. (D) Relative proportions across regions of putative glioma stem cells (GSCs), identified based on 9 published definitions/gene signatures.

while NE regions harbor glioma cells with potential nonpathological central nervous system (CNS) cell interactions and a landscape that mimics lower grade gliomas (with the exception of a relatively high rate of proliferative cells).

Regional Comparison of Putative Glioma Stem Cells

Glioma initiation, progression, invasion, and recurrence may be driven by specific cell populations that are potentially present in residual NE regions. These cells may have certain stem-like properties or specific copy number alterations contributing to their phenotypes.[34] While putative glioma stem cells (GSCs) have been well-studied, there is no universally accepted genomic or transcriptomic definition. To evaluate regional differences in putative GSC populations, we used 9 previously studied GSC gene signatures[12,16,28,29,32–34,40] and identified putative GSCs in our dataset (Figure 4D). There was significant heterogeneity in GSC fraction (mean 0%–38%). Comparing GSC proportion in CE versus NE yielded no consistent difference ($P > .05$ each). Importantly, all definitions revealed putative GSCs in NE regions. Overall, investigating these glioma populations with previously established roles in tumor initiation, propagation, invasion, and recurrence implicates residual NE regions as harboring critical populations that may serve as targets of adjuvant therapy.

Composition and Molecular Features of Nonmalignant Cell Populations in NE Regions

We next focused on regional differences in the tumor microenvironment. Using marker expression patterns and hierarchical clustering, we annotated nonmalignant clusters as astrocytes, oligodendrocytes, excitatory neurons, interneurons, endothelial cells, T cells, tumor-associated microglia, and tumor-associated macrophages (Figure 4A). We first examined cell type composition and noted that oligodendrocytes were the most represented cell type in all tumors except for Gr4-GBM-1, which had a neuronal majority (likely due to the biopsy sites' proximity to gray matter rather than white matter). This highlights the invasive nature of glioma, with malignant cells integrating into nonpathological CNS tissue. Comparing composition across regions revealed lower T cell proportions in NE for all tumors (mean 0.56% vs. 1.94%, paired *t*-test $P = .14$; Figure 4B). Given the low numbers of T cells, we were unable to meaningfully subclassify (ie, $CD4^+$, $CD8^+$, NK subsets). Consistent with previous reports,[19] the tumor-associated macrophage:microglia ratio was higher in the CE regions of all tumors except Gr4-GBM-2. We subjectively identified relatively increased proportions of nontumor CNS cells in NE regions (oligodendrocyte, neuron) versus tumor (using anti-EGFR as a proxy) via IHC analysis (Supplementary Figure 3). Consistent with our sequencing data, there is abundant staining for MBP in NE and CE areas, while there is very little to no staining for the T cell marker CD8. There is a greater level of anti-CD31 staining in CE, showing the hypervascularity of this region, and a greater level of staining for EGFR in CE, suggesting a greater tumor cell burden. There were no clear regional patterns in other cell type proportions.

We examined global and cell type-specific regional transcriptomic differences in nonmalignant cells by identifying differentially expressed genes (DEGs) in NE versus CE in the integrated dataset (Figure 4C and D). In oligodendrocytes, heat shock proteins (eg, *HSPA1A, HSPH1*) and the metabolic gene *ENOX2* were NE-enriched, while *VEGFA* was CE-enriched. In neurons, genes associated with hypoxic conditions (eg, *NGB*) and increased metabolism (eg, *MT-ATP6, MT-CO1, MT-CO2, MT-CYB*) were NE-enriched, while genes related to cell adhesion (eg, *CADM2, LAMA2, CDH18*) and neuronal function (eg, *DLG2, NRG3, CSMD1, PARK2*) were CE-enriched. In tumor-associated microglia, heat shock protein genes (eg, *HSPA1B, HSP90AA1, HSPH1*) were NE-enriched, and a gene associated with monocyte-to-macrophage differentiation (*CPM*) was CE-enriched. In tumor-associated macrophages, genes associated with interaction and reorganization of the extracellular matrix (eg, *TNS1, VIM, TRIO*) were CE-enriched. Lastly, genes involved in blood–brain barrier (BBB; eg, *CLDN11, PDGFRb*) were NE-enriched in nontumor cells overall.

We also assessed regional enrichment of functional pathways in nonmalignant cells using GSEA (Figure 4E). In oligodendrocytes, we observed upregulated HSF1 activity and downregulated Slit/Robo signaling[41] in NE. In neurons, we observed upregulation of oxidative phosphorylation and translation and downregulation of endothelin and neuron/synapse terms in NE. Evaluation of tumor-associated microglia demonstrated upregulation in metabolism and downregulation in immune function in NE, with tumor-associated macrophages interestingly exhibiting the opposite pattern. These cell-, gene-, and pathway-level analyses identify unique features of the nontumor microenvironment in NE regions, highlighted by decreased T cell fractions, possible region-specific tumor-associated microglia/macrophage phenotypes, and markers of cellular stress (eg, HSF1) in multiple cell types. Furthermore, these data suggest altered regulation of vascular integrity in NE regions, which may explain the limitation of gadolinium leakage from affected blood vessels and therefore lack of contrast enhancement in this region.[42]

Cell–cell Communication Networks in the NE Region Exhibit Differential Functional Wiring and Information Flow

Crosstalk between malignant cells and normal cells is a hallmark feature of cancer and is critical to tumor growth, invasion, and recurrence. To analyze cell–cell interaction (CCI) networks, we utilized CellChat[43] to build a CCI atlas for each tumor to examine general principles of cellular communication. The 5 high-grade gliomas were analyzed individually, with malignant and nonmalignant cells combined. We identified between 112 and 150 putatively active CCI pathways in each tumor out of 223 total pathways in the database. A total of 160 unique pathways were identified; 96 were detected in all tumors. We performed differential analysis to identify shared and patient-specific CCI differences between NE and CE (Figure 5A). We were unable to meaningfully study tumor subpopulations (ie,

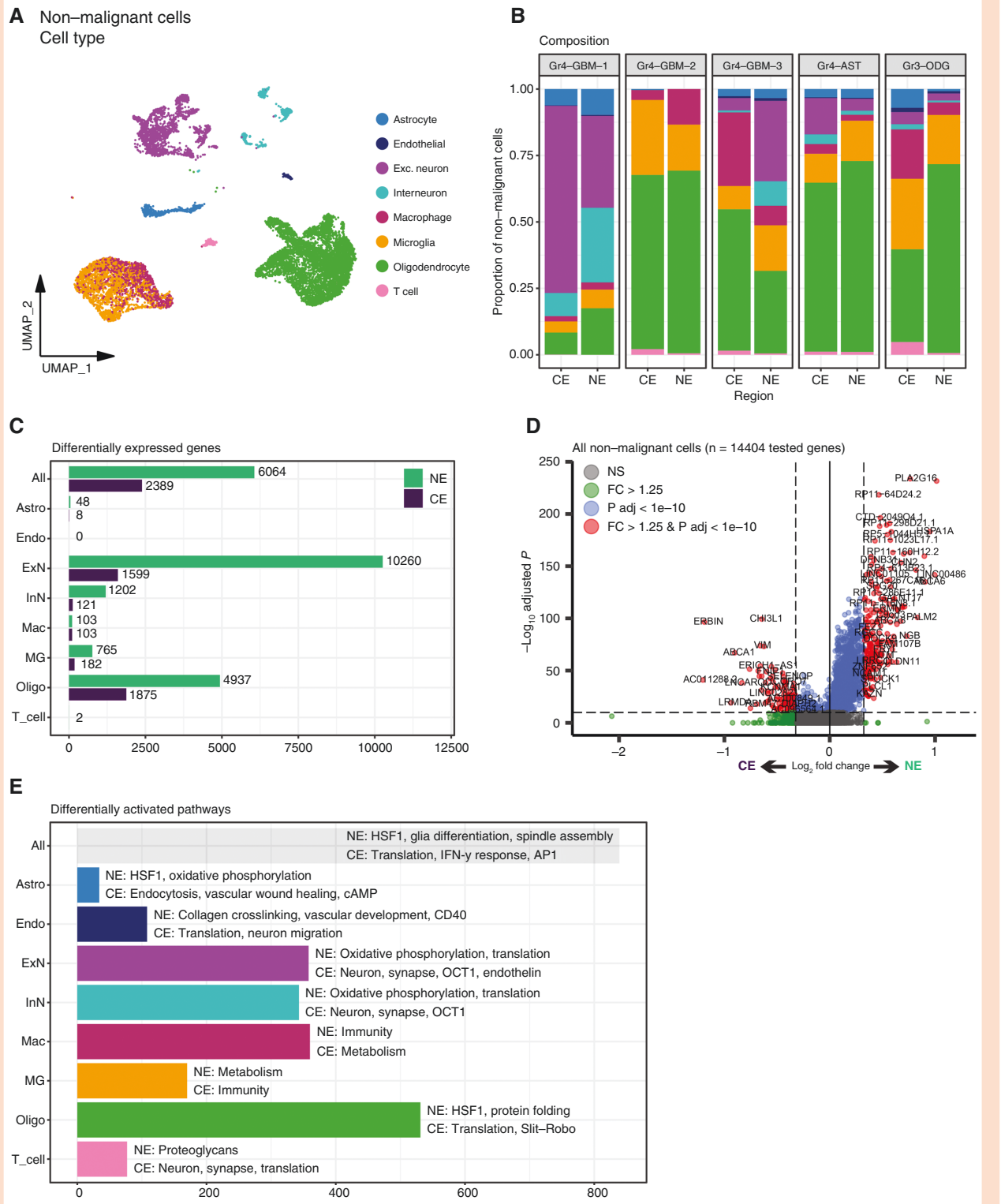

Figure 4. Altered nonmalignant cell microenvironment in NE region of high-grade gliomas. (A) UMAP representation of nonmalignant cells labeled by cell type. (B) Cell type composition of nonmalignant cells in the NE versus CE regions of each tumor. (C) Number of NE-enriched and CE-enriched differentially expressed genes (DEGs) in nonmalignant cell types. (D) Volcano plot depicting results of differential expression analysis in all nonmalignant cells combined, NE versus CE. (E) Number and summary of cell type-specific GSEA results using the identified DEGs with a combination of the GO Biological Process, Canonical Pathway, Oncogenic Pathway, and Transcription Factor Target databases. *(Astro = astrocytes, Endo = endothelial cells, ExN = excitatory neurons, InN = interneurons, Mac = tumor-associated macrophages, MG = tumor-associated microglia, Oligo = oligodendrocytes, T_cell = T cells).*

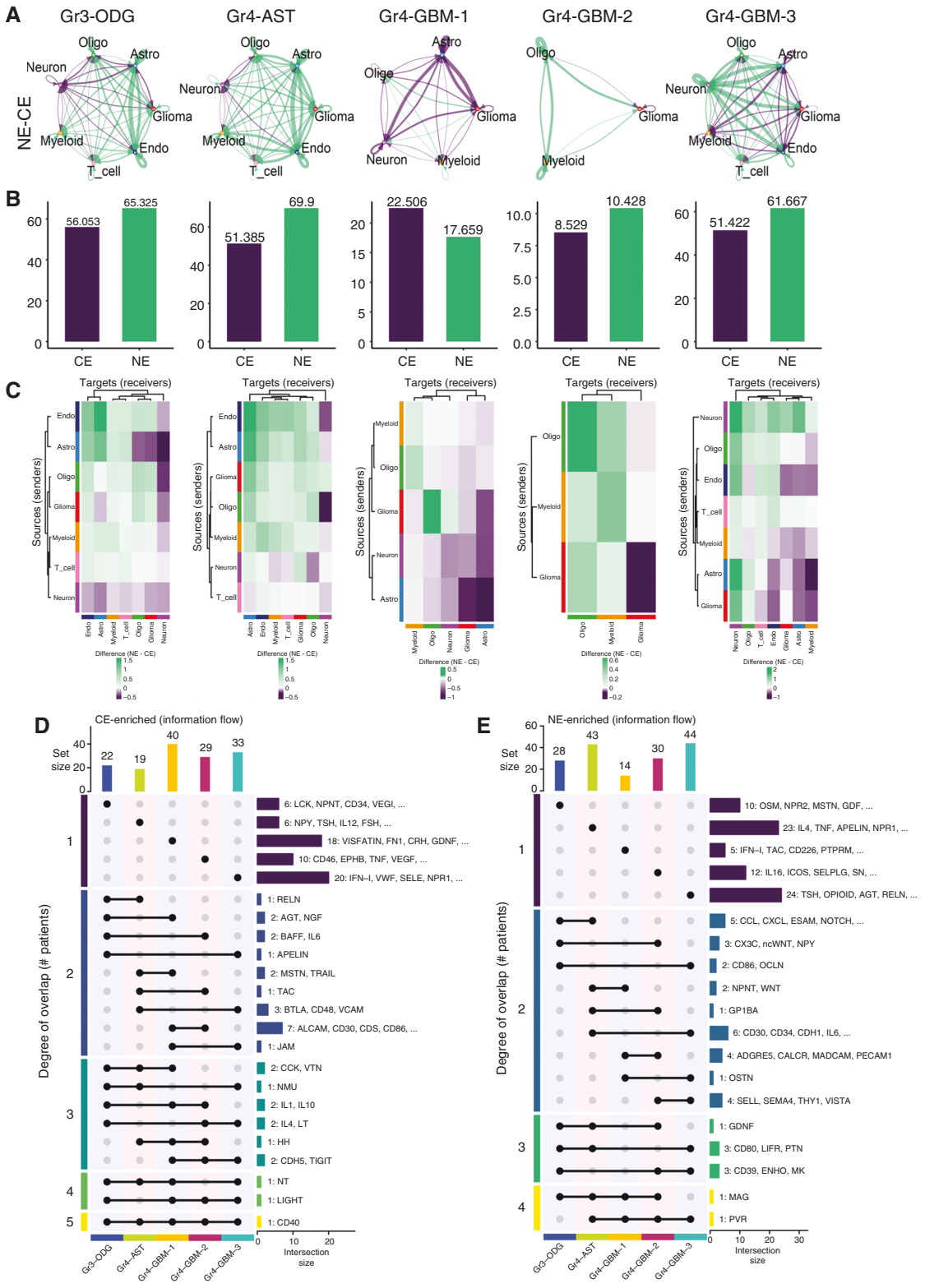

Figure 5. Regional differences in cell–cell interaction strength at the cell type level. (A) Differential interaction strength in NE versus CE for individual cell–cell interactions. Colors correspond to the region with stronger signaling, and line segment thickness corresponds to magnitude of regional difference. (B) Total interaction strength between NE and CE networks. (C) Heatmap of differential interaction strengths in NE versus CE among all possible cell type pairs, with rows being senders and columns being receivers of communication. Row and column dendrograms indicate similarity based on hierarchical clustering. UpSet plots depicting overlap of differential information flow enriched in (D) CE and (E) NE regions. Dots in each row indicate which tumor (degree of 1) or tumors (degree of 2+) comprise each group, and bars on the right indicate how many and which pathways are present exclusively in each group (ie, pathways can only be present in 1 row). Bars on the top indicate the number of regionally heterogeneous pathways in each tumor.

glioma cellular states) separately with any statistical significance given sample size constraints. Communication strength (ie, probability) was higher in NE for 4 of the 5 tumors (Figure 5B). In all tumors, glioma-to-oligodendrocyte interactions were upregulated in NE relative to CE (Figure 5C). In regard to specific communication pathways, CD40 signaling was CE-enriched in all tumors; NT and LIGHT/TNFSF14 were CE-enriched in 4 tumors (Figure 5D); and PVR/CD155 (invasion/infiltration) and MAG (myelin interaction) were NE-enriched in 4 tumors (Figure 5E). In the additional dataset of primary GBM, we found expression in NE regions of CD155 but no expression of MAG (Supplementary Figure 1E). We validated these findings using IHC, showing elevated CD155 and MAG in NE regions relative to CE regions (Supplementary Figure 4). Additional conserved CE-enriched pathways included immune (IL1, IL10, IL4, TIGIT) and endothelial (CDH5) mediators, and conserved NE-enriched pathways included heparin-binding growth factor pathways (MK, PTN) and microglial attraction (GDNF). Together, these findings highlight global and cell type-specific differences in the cellular communication landscape of NE regions compared to CE regions.

Discussion

In this study, we leveraged single-nucleus RNA sequencing and MRI-guided biopsy target selection to dissect spatial phenotypes in high-grade glioma. While prior studies have characterized cells in both NE and CE regions,[19,44] our approach has the advantage of being able to capture sufficient numbers of cells from each region to ascertain regional differences. With this in mind, we focused on characterizing these infiltrating NE regions on a single-cell level by taking MRI-guided samples of these areas during surgery. We confirmed there was a significant tumor burden beyond the CE region in all recurrent high-grade gliomas. Our model predicted that cells may exist multiple centimeters beyond the CE edge, potentially occurring in a portion of FLAIR hyperintensity surrounding the tumor. NE regions had similar levels of cycling cells and putative GSCs (using several definitions) as CE regions, suggesting these residual NE areas likely harbor propagators of progression and recurrence after gross total resection of CE tumor. This confirms previous studies identifying tumor burden using image-guided biopsies.[19,44]

We used cell-, gene-, pathway-, and interactome-level analyses to characterize both infiltrating tumor and microenvironment in the NE region. Although only one study in primary glioma utilized MRI-guided biopsies to determine NE and CE, other studies have examined somewhat analogous regional variations. Our own analysis of the image-based study, Darmanis et al.[19] indicates that there are regional differences in gene expression and cellular state composition that are consistent with previous findings in primary glioma. Minata et al.[45] identified higher MES-like cells in core regions and higher NPC-like cells in edge regions. Similarly, Gill et al.[46] identified that edge regions predominantly resemble the neural TCGA subtype, which may be a result of the ratio of tumor-to-nontumor CNS cells. However, it is unclear whether these previously described areas correlate to CE or NE regions. Our differential expression analysis in recurrent tumors showed upregulation of genes associated with lower grade tumors and downregulation of genes associated with proliferation/invasion in NE regions. Furthermore, the cycling cells of NE regions were almost exclusively OPC-like and NPC-like, consistent with previous data in primary GBM demonstrating more OPC-like and NPC-like cells in edge regions.[46] These latter findings suggest potential relationships between cellular states and MRI findings in that NPC-/OPC-like cells correlate with NE characteristics and low-grade biology, while MES-/AC-like cells correlate with CE characteristics and high-grade biology.

In regard to the tumor microenvironment, we highlight low levels of immune cells and relatively decreased tumor necrosis factor-related pathways (eg, CD40, LIGHT, TIGIT) in NE regions, suggesting a relative lack of immune response compared to CE. Our findings are consistent with other immunophenotyping studies that have found underrepresentation of T cells in NE regions.[47] In addition, we find several possible biological etiologies of NE characteristics: low levels of endothelial cells and upregulation of BBB proteins may restrict contrast extravasation; markers of hypoxic stress likely indicate future neovascularization; and signaling between glioma and nonpathological CNS cells may support active glioma interaction/infiltration along the NE edge of tumor. These microenvironment characteristics all provide biological insight into difficulty with immunotherapy, drug delivery, and surgical treatment.

Our study has several limitations. Due to the limited number of tumors in each pathological designation, we cannot confidently draw statistical conclusions between types of tumors. Furthermore, the specimens from the NE region in each tumor were limited to a single site given the need to limit sampling of potential nonpathologic neural tissue, leaving open the possibility that different portions of the NE regions behave differently. Lastly, while studying recurrent gliomas allowed comprehensive characterization and comparison with findings in primary gliomas, certain conclusions are limited in their generalizability to primary tumors.

Overall, we believe this study highlights the importance of acquiring and studying NE regions of glioma. We make this conclusion for the following reasons: (1) there exists a significant tumor burden in NE regions; (2) NE tumor cells are actively dividing and harbor putative GSC markers; and (3) there exists differential gene expression compared to heavily studied CE regions. We have highlighted potential biological mediators of interest specific to NE regions, like PVR/CD155 and MAG, through RNA and protein analysis. This has consequences for both surgical and molecular treatment, giving a biological underpinning for supramaximal resection when possible. We recognize that complete resection is highly unlikely given functional eloquence; therefore, we look to study pathways critical to the function of NE cells and adapt previous in vitro and in vivo patient-derived models to NE regions of glioblastoma as a fundamental change in strategy for developing molecular therapy for postsurgical glioblastoma.

Supplementary material

Supplementary material is available online at *Neuro-Oncology* (https://academic.oup.com/neuro-oncology).

Keywords

contrast enhancing | glioblastoma | magnetic resonance imaging | non-enhancing

Funding

This work was supported by the Dr. Miriam and Sheldon G. Adelson Medical Research Foundation (H.I.K., R.K., S.A.G.); NIH grants P50 CA211015 (H.I.K., B.E., D.G., W.Y., L.L.), R01 NS121617 (H.I.K.), and F31 MH122205 (K.K.T.); the Broad Stem Cell Research Center (K.S.P., S.D.M.); the UC President's Postdoctoral Fellowship Program (A.G.A.); the NIH National Center for Advancing Translational Science UCLA CTSI Grant KL2TR001882 (K.S.P.), and Neurosurgical Research Education Fund Young Clinical Investigator Award (K.S.P).

Conflict of interest statement

The authors have declared that no conflict of interest exists.

Authorship statement

K.S.P.: study conception; acquiring data; analyzing data; writing/revising manuscript. K.K.T.: acquiring data; analyzing data; figure generation; writing/revising manuscript. R.K.: analyzing data; figure generation. L.D.: analyzing data, figure generation. A.A.: analyzing data; writing/revising manuscript. S.D.M.: analyzing data; writing/revising manuscript. T.P.: acquiring data; analyzing data. A.H.: acquiring data; analyzing data. V.S.: analyzing data; study supervision. L.M.L.: acquiring data; revising manuscript, study supervision. A.C.W.: acquiring data; revising manuscript, study supervision. W.Y.: acquiring data; revising manuscript, study supervision. D.H.G.: acquiring data; revising manuscript, study supervision. I.N.: revising manuscript, study supervision. S.A.G.: revising manuscript, study supervision. R.G.E.: study conception; acquiring data; revising manuscript, study supervision. B.M.E.: study conception; acquiring data; analyzing data; revising manuscript, study supervision. H.I.K.: study conception; acquiring data; analyzing data; writing/revising manuscript, study supervision. First authorship order was determined by corresponding author by individual contribution.

References

1. Brown TJ, Brennan MC, Li M, et al. Association of the extent of resection with survival in glioblastoma: a systematic review and meta-analysis. *JAMA Oncol.* 2016;2(11):1460–1469.
2. Marko NF, Weil RJ, Schroeder JL, et al. Extent of resection of glioblastoma revisited: personalized survival modeling facilitates more accurate survival prediction and supports a maximum-safe-resection approach to surgery. *J Clin Oncol.* 2014;32(8):774–782.
3. Wen PY, Kesari S. Malignant gliomas in adults. *N Engl J Med.* 2008;359(5):492–507.
4. Sanai N, Polley MY, McDermott MW, Parsa AT, Berger MS. An extent of resection threshold for newly diagnosed glioblastomas. *J Neurosurg.* 2011;115(1):3–8.
5. Ellingson BM, Abrey LE, Nelson SJ, et al. Validation of postoperative residual contrast-enhancing tumor volume as an independent prognostic factor for overall survival in newly diagnosed glioblastoma. *Neuro Oncol.* 2018;20(9):1240–1250.
6. Bette S, Barz M, Huber T, et al. Retrospective analysis of radiological recurrence patterns in glioblastoma, their prognostic value and association to postoperative infarct volume. *Sci Rep.* 2018;8(1):4561.
7. Erdem-Eraslan L, van den Bent MJ, Hoogstrate Y, et al. Identification of patients with recurrent glioblastoma who may benefit from combined bevacizumab and CCNU therapy: a report from the BELOB Trial. *Cancer Res.* 2016;76(3):525–534.
8. Taal W, Oosterkamp HM, Walenkamp AME, et al. Single-agent bevacizumab or lomustine versus a combination of bevacizumab plus lomustine in patients with recurrent glioblastoma (BELOB trial): a randomised controlled phase 2 trial. *Lancet Oncol.* 2014;15(9):943–953.
9. Brandes AA, Finocchiaro G, Zagonel V, et al. AVAREG: a phase II, randomized, noncomparative study of fotemustine or bevacizumab for patients with recurrent glioblastoma. *Neuro Oncol.* 2016;18(9):1304–1312.
10. Cloughesy TF, Mochizuki AY, Orpilla JR, et al. Neoadjuvant anti-PD-1 immunotherapy promotes a survival benefit with intratumoral and systemic immune responses in recurrent glioblastoma. *Nat Med.* 2019;25(3):477–486.
11. Patel AP, Tirosh I, Trombetta JJ, et al. Single-cell RNA-seq highlights intratumoral heterogeneity in primary glioblastoma. *Science.* 2014;344(6190):1396–1401.
12. Venteicher AS, Tirosh I, Hebert C, et al. Decoupling genetics, lineages, and microenvironment in IDH-mutant gliomas by single-cell RNA-seq. *Science.* 2017;355(6332):eaai8478.
13. Neftel C, Laffy J, Filbin MG, et al. An integrative model of cellular states, plasticity, and genetics for glioblastoma. *Cell.* 2019;178(4):835–849.e21.
14. Tirosh I, Venteicher AS, Hebert C, et al. Single-cell RNA-seq supports a developmental hierarchy in human oligodendroglioma. *Nature.* 2016;539(7628):309–313.
15. Weng Q, Wang J, Wang J, et al. Single-cell transcriptomics uncovers glial progenitor diversity and cell fate determinants during development and gliomagenesis. *Cell Stem Cell.* 2019;24(5):707–723.e8.
16. Wang L, Babikir H, Müller S, et al. The phenotypes of proliferating glioblastoma cells reside on a single axis of variation. *Cancer Discov.* 2019;9(12):1708–1719.
17. Lan X, Jörg DJ, Cavalli FMG, et al. Fate mapping of human glioblastoma reveals an invariant stem cell hierarchy. *Nature.* 2017;549(7671):227–232.
18. Abdelfattah N, Kumar P, Wang C, et al. Single-cell analysis of human glioma and immune cells identifies S100A4 as an immunotherapy target. *Nat Commun.* 2022;13(1):767.

19. Darmanis S, Sloan SA, Croote D, et al. Single-cell RNA-Seq analysis of infiltrating neoplastic cells at the migrating front of human glioblastoma. *Cell Rep.* 2017;21(5):1399–1410.
20. Ellingson BM, Bendszus M, Boxerman J, et al.; Jumpstarting Brain Tumor Drug Development Coalition Imaging Standardization Steering Committee. Consensus recommendations for a standardized brain tumor imaging protocol in clinical trials. *Neuro-Oncol.* 2015;17(9):1188–1198.
21. Cox RW. AFNI: software for analysis and visualization of functional magnetic resonance neuroimages. *Comput Biomed Res.* 1996;29(3):162–173.
22. Stupp R, Mason WP, van den Bent MJ, et al.; European Organisation for Research and Treatment of Cancer Brain Tumor and Radiotherapy Groups. Radiotherapy plus concomitant and adjuvant temozolomide for glioblastoma. *N Engl J Med.* 2005;352(10):987–996.
23. Bankhead P, Loughrey MB, Fernández JA, et al. QuPath: open source software for digital pathology image analysis. *Sci Rep.* 2017;7(1):16878.
24. Heinemann J. Cluster analysis of untargeted metabolomic experiments. In: Baidoo E, ed. *Microbial Metabolomics*. vol. 1859. New York, NY: Humana Press; 2019:275–285.
25. Stuart T, Butler A, Hoffman P, et al. Comprehensive integration of single-cell data. *Cell.* 2019;177(7):1888–1902.e21.
26. Hao Y, Hao S, Andersen-Nissen E, et al. Integrated analysis of multimodal single-cell data. *Cell.* 2021;184(13):3573–3587.e29.
27. Neftel C, Laffy J, Filbin MG, et al. An integrative model of cellular states, plasticity, and genetics for glioblastoma. *Cell.* 2019;178(4):835–849.e21.
28. Bhaduri A, Di Lullo E, Jung D, et al. Outer radial glia-like cancer stem cells contribute to heterogeneity of glioblastoma. *Cell Stem Cell.* 2020;26(1):48–63.e6.
29. Xie XP, Laks DR, Sun D, et al. Quiescent human glioblastoma cancer stem cells drive tumor initiation, expansion, and recurrence following chemotherapy. *Dev Cell.* 2022;57(1):32–46.e8.
30. Couturier CP, Ayyadhury S, Le PU, et al. Single-cell RNA-seq reveals that glioblastoma recapitulates a normal neurodevelopmental hierarchy. *Nat Commun.* 2020;11(1):3406.
31. Wang Q, Hu B, Hu X, et al. Tumor evolution of glioma-intrinsic gene expression subtypes associates with immunological changes in the microenvironment. *Cancer Cell.* 2017;32(1):42–56.e6.
32. Antonica F, Santomaso L, Pernici D, et al. A slow-cycling/quiescent cells subpopulation is involved in glioma invasiveness. *Nat Commun.* 2022;13(1):4767.
33. Suvà ML, Rheinbay E, Gillespie SM, et al. Reconstructing and reprogramming the tumor-propagating potential of glioblastoma stem-like cells. *Cell.* 2014;157(3):580–594.
34. Suvà ML, Tirosh I. The glioma stem cell model in the era of single-cell genomics. *Cancer Cell.* 2020;37(5):630–636.
35. Jin S, Guerrero-Juarez CF, Zhang L, et al. Inference and analysis of cell-cell communication using CellChat. *Nat Commun.* 2021;12(1):1088.
36. Ellingson BM, Aftab DT, Schwab GM, et al. Volumetric response quantified using T1 subtraction predicts long-term survival benefit from cabozantinib monotherapy in recurrent glioblastoma. *Neuro Oncol.* 2018;20(10):1411–1418.
37. Williams MV, Denekamp J, Fowler JF. A review of alpha/beta ratios for experimental tumors: implications for clinical studies of altered fractionation. *Int J Radiat Oncol Biol Phys.* 1985;11(1):87–96.
38. Louis DN, Perry A, Wesseling P, et al. The 2021 WHO classification of tumors of the central nervous system: a summary. *Neuro Oncol.* 2021;23(8):1231–1251.
39. Schaub C, Kebir S, Junold N, et al. Tumor growth patterns of MGMT-non-methylated glioblastoma in the randomized GLARIUS trial. *J Cancer Res Clin Oncol.* 2018;144(8):1581–1589.
40. Couturier CP, Ayyadhury S, Le PU, et al. Single-cell RNA-seq reveals that glioblastoma recapitulates a normal neurodevelopmental hierarchy. *Nat Commun.* 2020;11(1):3406.
41. Tong M, Jun T, Nie Y, Hao J, Fan D. The role of the slit/robo signaling pathway. *J Cancer.* 2019;10(12):2694–2705.
42. Treiber JM, Steed TC, Brandel MG, et al. Molecular physiology of contrast enhancement in glioblastomas: an analysis of the Cancer Imaging Archive (TCIA). *J Clin Neurosci.* 2018;55:86–92.
43. Jin S, Guerrero-Juarez CF, Zhang L, et al. Inference and analysis of cell-cell communication using CellChat. *Nat Commun.* 2021;12(1):1088.
44. Gill BJ, Pisapia DJ, Malone HR, et al. MRI-localized biopsies reveal subtype-specific differences in molecular and cellular composition at the margins of glioblastoma. *Proc Natl Acad Sci USA.* 2014;111(34):12550–12555.
45. Minata M, Audia A, Shi J, et al. Phenotypic plasticity of invasive edge glioma stem-like cells in response to ionizing radiation. *Cell Rep.* 2019;26(7):1893–1905.e7.
46. Gill BJ, Pisapia DJ, Malone HR, et al. MRI-localized biopsies reveal subtype-specific differences in molecular and cellular composition at the margins of glioblastoma. *Proc Natl Acad Sci U S A.* 2014;111(34):12550–12555.
47. Grabowski MM, Watson DC, Chung K, et al. Spatial immunosampling of MRI-defined glioblastoma regions reveals immunologic fingerprint of non-contrast enhancing, infiltrative tumor margins. Version 1. *medRxiv.* 2023;(1). doi:10.1101/2023.03.09.23285970.